Surface Variation Modeling by Fusing Multiresolution Spatially Nonstationary Data Under a Transfer Learning Framework

Jie Ren
Department of Industrial and Manufacturing Engineering,
Florida A&M University-Florida State University College of Engineering,
Tallahassee, FL 32310

Hui Wang[1]
Department of Industrial and Manufacturing Engineering,
Florida A&M University-Florida State University College of Engineering,
Tallahassee, FL 32310
e-mail: hwang10@fsu.edu

High-definition metrology (HDM) has gained significant attention for surface quality inspection since it can reveal spatial surface variations in detail. Due to its cost and durability, such HDM measurements are occasionally implemented. The limitation creates a new research opportunity to improve surface variation characterization by fusing the insights gained from limited HDM data with widely available low-resolution surface data during quality inspections. A useful insight from state-of-the-art research using HDM is the revealed relationship and positive correlation between surface height and certain measurable covariates, such as material removal rate (MRR). Such a relationship was assumed spatially constant and integrated with surface measurements to improve surface quality modeling. However, this method encounters challenges when the covariates have nonstationary relationships with the surface height over different surface areas, i.e., the covariate-surface height relationship is spatially varying. Additionally, the nonstationary relationship can only be captured by HDM, adding to the challenge of surface modeling when most training data are measured at low resolution. This paper proposes a transfer learning (TL) framework to deal with these challenges by which the common information from a spatial model of an HDM-measured surface is transferred to a new surface where only low-resolution data are available. Under this framework, the paper develops and compares three surface models to characterize the nonstationary relationship including two varying coefficient-based spatial models and an inference rule-based spatial model. Real-world case studies were conducted to demonstrate the proposed methods for improving surface modeling. [DOI: 10.1115/1.4041425]

Keywords: surface variation modeling, data fusion, nonstationary process, transfer learning, varying coefficient models, adaptive network-based fuzzy inference system (ANFIS)

1 Introduction

Surface shape variations greatly affect the quality of the products. For example, in powertrain manufacturing, significant surface shape variations may lead to functional performance problems such as leakage or cam bore distortion, resulting in high scrap rates and wastes [1–3]. To check the quality of surfaces, a manufacturing plant usually employs a combination of several metrology systems with different resolutions such as coordinate measuring machine (CMM) for overall surface shape and a profilometer for surface roughness inspection at several local areas (Fig. 1). The surface inspection using these low-definition metrology (LDM) systems may fail to detect abnormal regions in unmeasured areas. As a result, the characterization of surface shape spatial variations in high resolution is needed for high-precision surface manufacturing. Utilizing high resolution (high density) data, comprehensive analysis can be conducted for spatial surface quality assessment, such as engineering surface classification [4], defect detection [5], and leakage modeling [2,3]. To obtain the high resolution data, common methods in prior research utilized the interpolation/extrapolation of the surface measurement, such as least squares [6], B-spline methods [7–9], grid fit through triangulation [10], and spatial Gaussian process based method [11–14] to model the surface variations in high resolution. The modeling framework in prior research is shown in Fig. 2(*a*). However, the modeling accuracy of these interpolation/extrapolation methods is highly dependent on the density of measurement data. Current surface measurement strategy (see Fig. 1) does not provide sufficient density of local data for these methods to make accurate surface estimations, potentially limiting the applications of this line of approaches in high-precision manufacturing.

With the advancement of high-definition metrology (HDM) systems in the recent years, new research opportunities emerge for improving surface variation models and characterization. The

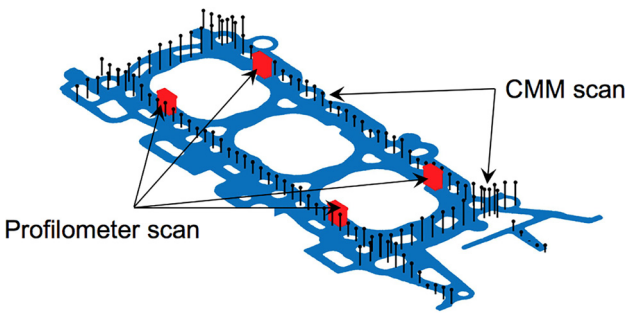

Fig. 1 Profilometer measurements on surface roughness and CMM measurements on surface flatness

[1]Corresponding author.

Manuscript received January 15, 2018; final manuscript received September 6, 2018; published online October 10, 2018. Assoc. Editor: Laine Mears.

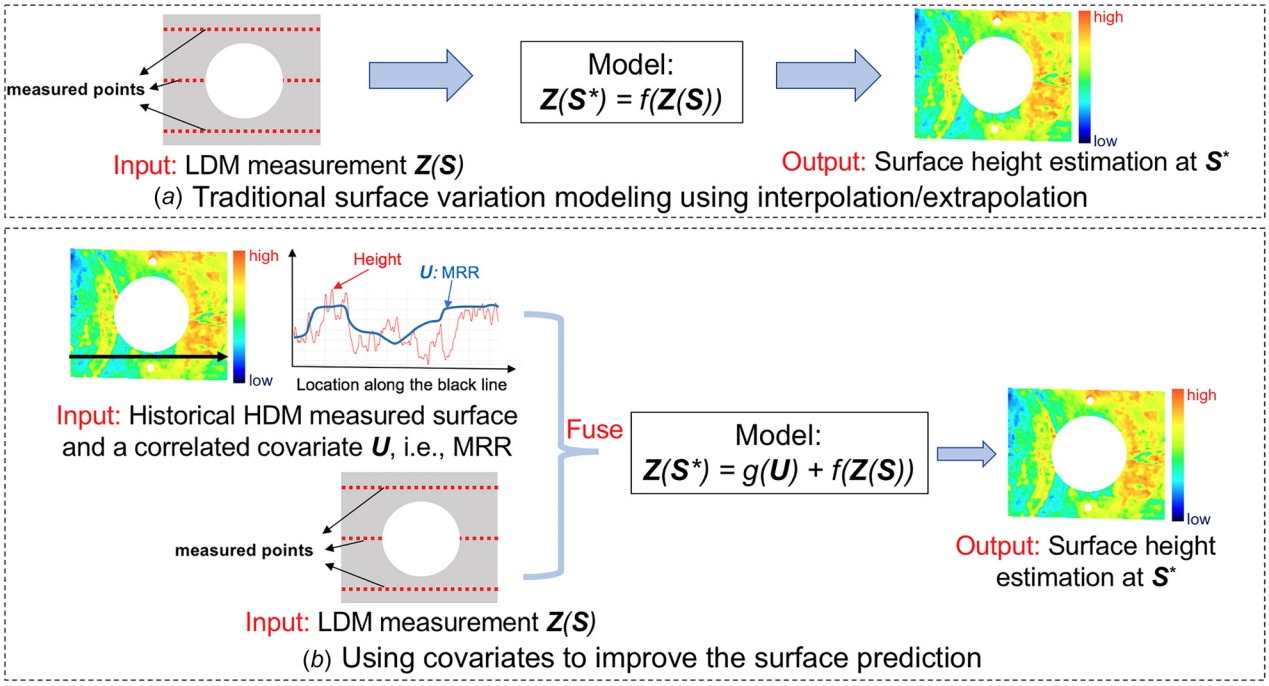

Fig. 2 An outline of the research problem formulation for HDM-based surface variation modeling

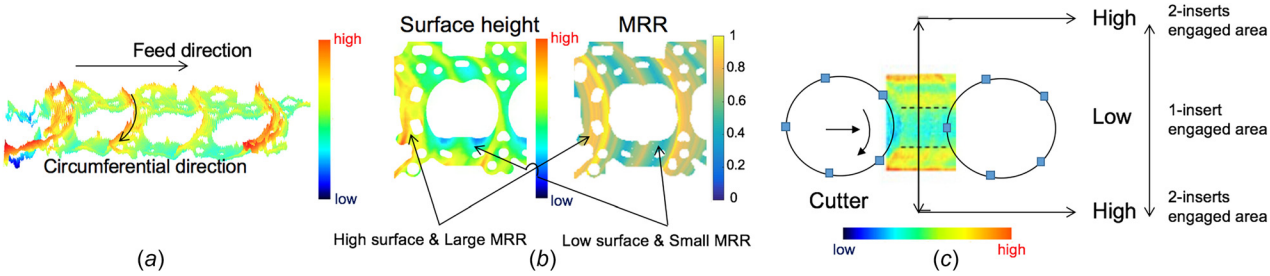

Fig. 3 Correlation between process variables and surface height: (*a*) two directions while cutting; (*b*) normalized MRR and its relation with surface variation; and (*c*) cutter insert engagement with surface and its impact on surface height

HDM system, such as a laser holographic interferometer, can reveal spatial surface variations in great detail over an area up to $300 \times 300\,\text{mm}^2$ within minutes. Nevertheless, the HDM system has not frequently been employed in many plants to inspect surfaces during routine quality check due to its high cost and durability of its optical system. As such, the HDM surface data are available for very limited parts, and a majority of surface data are still collected by in-plant LDM systems. Very recent research has been developed to fuse the in-plant LDM measurements with historical HDM measurements by extracting surface variation patterns that are correlated to certain measurable variables from historical HDM data and using them as covariates to guide the model improvement of LDM-measured surfaces. For example, prior research [1,15] has reported a positive correlation between surface height variation along the cutter's feed direction and a covariate, i.e., material removal rate (MRR, the material removal volume per cutter revolution) in a surface milling process as shown in Fig. 3(*b*). Additionally, the surface variation along the circumferential direction is correlated to the number of cutter insert engaged in the cutting process (Fig. 3(*c*)). Such correlation is induced by axial cutting force variation, which is reflected by the changes of MRR and cutter insert engagement. Using these covariates, Suriano et al. [16] proposed a regression-Kriging based spatial surface model that greatly improved surface shape variation modeling. Shao et al. [17] developed a multitask learning based algorithm to train the regression-Kriging based spatial model for improving the modeling accuracy of data-lacking processes. Du and Fei [18] proposed a co-Kriging based multivariate spatial model, which considered the correlation between surface height and vibration.

In summary, the *research problem* for HDM-based surface modeling is to improve the estimation and characterization of surface variations in high resolution by fusing the information obtained from historical HDM data, which have limited the availability for quality checks, with in-plant LDM measurements, which are implemented for all inspection parts. As shown in Fig. 2(*b*), historical HDM measurements reveal the correlation between surface height and certain variables (covariates) denoted by $\boldsymbol{U}$, such as MRR. Such a relationship can be modeled by a function $g(\boldsymbol{U})$, which is usually assumed a linear form. LDM data contain surface measurements $\boldsymbol{Z}$ at locations $\boldsymbol{S}$. The locations where surface heights are to be estimated are denoted by $\boldsymbol{S}^*$. The surface estimations on $\boldsymbol{S}^*$, i.e., $\boldsymbol{Z}(\boldsymbol{S}^*)$, are made via an additive model that consists of two components. The first component $g(\boldsymbol{U})$ characterizes the covariates $\boldsymbol{U}$ induced surface variations. The second one $f(\boldsymbol{Z}(\boldsymbol{S}))$ is an interpolation/extrapolation method, such as

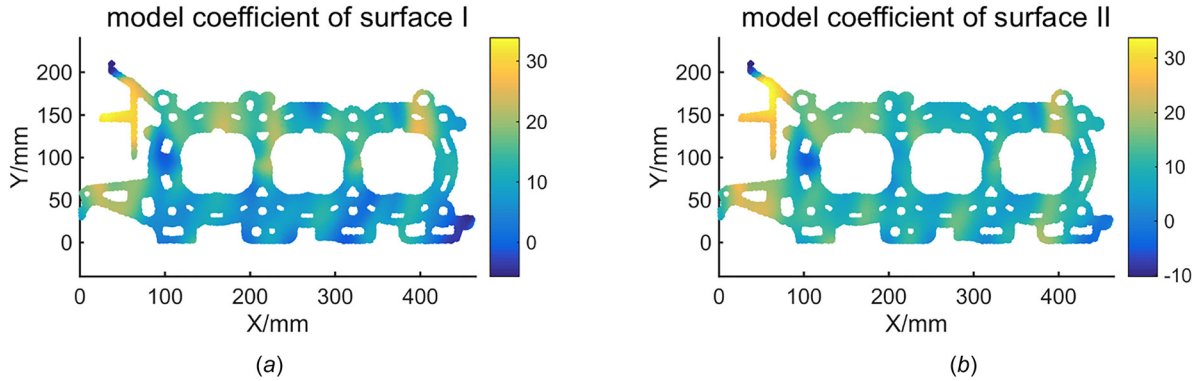

Fig. 4 Varying model coefficients of two engine head surfaces: (*a*) coefficient c_1 of surface I and (*b*) coefficient c_1 of surface II

Table 1 Regression results for validating the spatially varying coefficients (nonstationarity)

Local regression	Parameter	Minimum	First quartile	Second quartile	Third quartile	Maximum
Surface I	c_1	−5.65	6.77	10.28	15.05	33.85
	Adjusted R^2	0.82				
Surface II	c_1	−10.21	7.46	9.71	13.13	33.72
	Adjusted R^2	0.74				
Global regression	**Parameter**	**Estimated value**	**Standard error**	***p* value**		
Surface I	c_1	8.54	0.016	0		
	Adjusted R^2	0.13				
Surface II	c_1	9.91	0.017	0		
	Adjusted R^2	0.16				

a zero-mean Gaussian process model, aiming to characterize the surface variations that are not considered in $g(\boldsymbol{U})$. The development of the appropriate form of $g(\boldsymbol{U})$ and how the coefficients of $g(\boldsymbol{U})$ are estimated play critical roles in this line of research.

The fusion method as mentioned earlier using covariates has achieved great success; however, these methods have a limitation that is the relationship between covariates and surface height is assumed to be constant (stationary) over the entire surface areas, i.e., the coefficients of $g(\boldsymbol{U})$ are spatially constant. In many scenarios, this assumption does not hold. Figure 4 shows an example of comparing the surface height-covariate relationship for two automotive engine head deck faces, which were measured by HDM. The result shows that such a relationship for each surface is spatially varying (spatial nonstationary), i.e., the coefficient c_1 of the linear model, $Z = c_0 + c_1\text{MRR} + \text{error}$, is spatially varying. The estimated coefficient c_1 of the two surfaces is displayed as a color map in Fig. 4, which exhibits similar spatially varying patterns. The statistical summaries of the estimated coefficients are shown in Table 1. The results show that a global linear regression assumes spatially constant coefficients and leads to a poor estimation, i.e., $R^2 = 0.13$ and 0.16, respectively. By contrast, a local linear regression with spatially varying coefficients yields significantly improved results, i.e., $R^2 = 0.82$ and 0.74, respectively. The analysis of real-world engine head data demonstrates that it is necessary to consider a nonstationary relationship between covariates and surface height for surface variation modeling. According to Cheng et al.'s review of nonstationary processes [19], the nonstationarity in this paper can be treated as "arbitrary variation with either gradual or abrupt change" type of nonstationarity.

In summary, the *research gaps* for the surface variation modeling are as follows:

- There is a lack of surface modeling methods that consider the nonstationary relationship between the covariate and the surface height as revealed in Fig. 4. Current methods fusing the multiresolution measurements rely on the assumption of a static relationship, which averages out the spatial variations even when the relationship is nonstationary, thus affecting the accurate characterization of surface variations.
- There is a lack of methods that can effectively capture the nonstationary relationship based on the surface data measured by LDM. In prior research, capturing the nonstationarity as described earlier is achieved by HDM data. Methods are needed to transfer the knowledge of nonstationarity from historical HDM data with limited availability to the machined surfaces mostly measured by LDM.

This paper tackles the research gaps above for improving surface variation estimations. To address the first research gap, this paper proposes and compares three different models that are able to characterize either gradual or abrupt nonstationarity. To address the second research gap, this paper employs transfer learning (TL) approach. Transfer learning is to improve the modeling of a data-lacking process with the assistance of other similar-but-not-identical processes (a survey of transfer learning can be found in Ref. [20]). As can be seen from Fig. 4, the two surfaces exhibit similar-but-not-identical spatial patterns of varying coefficients, which motivates us to employ transfer learning technique for transferring useful common nonstationarity information from historical HDM measured surfaces to LDM measured surfaces. To achieve the transfer, this paper proposes regularization (penalty) based transfer learning methods for the three models to account for the similarity in the model coefficients of different surfaces.

The remainder of the paper is organized as follows. Section 2 presents three transfer learning enabled surface variation models. Section 3 presents two real-world case studies to demonstrate the advantages of transfer learning enabled methods over the selected prior commonly used methods. Conclusions are summarized in Sec. 4.

2 Transfer Learning Enabled Surface Variation Model

In this section, we proposed three different methods to enable the characterization of the nonstationary relationship between the covariate and the surface height and proposed penalized methods to facilitate the knowledge transfer from historical HDM data to the modeling of LDM measured surfaces. The three surface variation models in this paper share the same way decomposing the surface variations, i.e., the surface variations are decomposed into two main parts, including (1) covariates (e.g., MRR and the number of cutter insert engagement) induced surface variations that are characterized by the nonstationary relationship between the covariate and the surface height; and (2) spatially correlated surface variations characterized by a Gaussian process model. The model can be represented by the following equation:

$$Z(s) = g(\boldsymbol{U}(s)) + \mathrm{GP}(s) + \varepsilon(s) \tag{1}$$

where $Z(s)$ is the surface height at location s; $\boldsymbol{U}(s)$ is a vector representing the values of covariates at location s; g represents the model characterizing the nonstationary relationship of covariates ($\boldsymbol{U}$)-surface height ($\boldsymbol{Z}$); GP represents a zero mean Gaussian process, characterizing the autocorrelated residual variations of the surface; and $\varepsilon(s)$ is noise with i.i.d. $N \sim (0, \tau^2)$, where τ^2 determines the noise variance, i.i.d. means independent and identically distributed.

The proposed three models differ in the $g(\boldsymbol{U}(s))$ part of Eq. (1), which are (a) point-wise local model via geographically weighted regression (GWR) (Sec. 2.1), (b) region-wise model via spatial partition (Sec. 2.2), and (c) inference rule based model with fuzzy region boundaries (Sec. 2.3). The three models can capture the nonstationary patterns with abrupt or gradual changes in the covariate-surface height relationship.

It should be noted that the GP part of Eq. (1) is not the only choice for characterizing the autocorrelated residual variations. Other types of the Gaussian process model, e.g., additive Gaussian process model [21] or Gaussian Markov random field model [22], can also be employed. These Gaussian process models differ in the structure of covariance function and might be suitable for different situations. For the rest of the papers, we stay with the regular GP model.

2.1 Varying Coefficient Local Regression Based Spatial Model.

This section presents a point-wise local regression model with spatially varying coefficients to characterize the covariates induced surface variations. The local regression model refers to GWR [23], which fits a regression model at each location, thus capturing the spatial nonstationarity. In this case, the surface variations can be modeled as follows:

$$Z(s) = \boldsymbol{U}(s)\boldsymbol{\Gamma}(s) + \mathrm{GP}(s) + \varepsilon(s) \tag{2}$$

where $\boldsymbol{U}(s)\boldsymbol{\Gamma}(s)$ is the GWR model with location-dependent coefficient $\boldsymbol{\Gamma}(s)$.

In Sec. 2.1.1, we first review the GWR model and further propose transfer learning based geographically weighted regression (tl-GWR). Parameter estimation for the surface variation model, Eq. (2), is also discussed.

2.1.1 Review of the Geographically Weighted Regression. Geographically weighted regression allows the coefficients of the model to vary locally (point-wise), thereby characterizing a spatially nonstationary relationship. As an illustration, we assume that a dependent variable $\boldsymbol{O}$ and m independent variables $\boldsymbol{V}$ at the same N locations (the dimension of $\boldsymbol{O}$ and $\boldsymbol{V}$ is $N \times 1$ and $N \times m$, respectively) can be modeled via a GWR model as follows:

$$O(s) = \boldsymbol{V}(s)\boldsymbol{\Theta}(s) + \eta(s) \tag{3}$$

where $\boldsymbol{\Theta}(s)$ indicates that the coefficients $\boldsymbol{\Theta}$ are to be estimated at a location s; and η stands for normally distributed white noise. The dimensions of $O(s)$, $\boldsymbol{V}(s)$, and $\boldsymbol{\Theta}(s)$ are 1×1, $1 \times m$, and $m \times 1$, respectively.

To allow the coefficients $\boldsymbol{\Theta}$ to be spatially varying, the estimation of $\boldsymbol{\Theta}$ at location s can be solved via a weighting scheme as follows:

$$\boldsymbol{\Theta}(s) = (\boldsymbol{V}^T\boldsymbol{W}^g(s)\boldsymbol{V})^{-1}\boldsymbol{V}^T\boldsymbol{W}^g(s)\boldsymbol{O} \tag{4}$$

where $\boldsymbol{W}^g(s)$ is a diagonal weight matrix for location s with dimension of $N \times N$. The weights are chosen in a way such that those observations near s have more influence on the result. A Gaussian weight function is commonly used as follows:

$$w_i^g = e^{\frac{-d_i^2}{h^2}} \tag{5}$$

where w_i^g is the weight for observation at location i; d_i is the distance between location i and s; and h is the bandwidth that determines the degree of weight decline when distance increases. The value of h is usually determined by grid searching the optimal bandwidth with the best cross-validation value (see Ref. [23]). The coefficients $\boldsymbol{\Theta}$ are to be estimated for every locations of interest, thus exhibiting the spatial variability due to the weighting scheme.

2.1.2 Development of Transfer-Learning-Based Geographically Weighted Regression. For surfaces with only LDM measurements, conducting GWR for every locations of interest (to be estimated locations) cannot be accurate because the measurements are sparse and might be far away from the locations of interest. Considering the similar spatial nonstationarity of two surfaces shown in Fig. 4, this section proposes a regularized transfer learning enabled GWR model to estimate the spatially varying coefficients for the target surface measured only by LDM. The regularized transfer learning algorithm is proposed as follows:

$$\hat{\boldsymbol{\Theta}}(s) = \arg\min \frac{1}{2}(\boldsymbol{O} - \boldsymbol{V}\boldsymbol{\Theta}(s))^{\mathrm{T}}\boldsymbol{W}^g(s)(\boldsymbol{O} - \boldsymbol{V}\boldsymbol{\Theta}(s)) + \frac{1}{2}\lambda_g\|\boldsymbol{\Theta}(s) - \boldsymbol{\Theta}_0(s)\|_2^2 \tag{6}$$

where $\|\boldsymbol{\Theta}(s) - \boldsymbol{\Theta}_0(s)\|_2^2 = (\boldsymbol{\Theta}(s) - \boldsymbol{\Theta}_0(s))^{\mathrm{T}}(\boldsymbol{\Theta}(s) - \boldsymbol{\Theta}_0(s))$ (L_2 regularization, see Ref. [24]); $\Theta_0(s)$ is the parameter estimated by Eq. (4) for the HDM measured surface at location s; λ_g is a tuning parameter for the L_2 regularization; and $W(s)$ is a weight matrix calculated via LDM data using the same weight function with HDM measured surface. The solution to Eq. (6) is given by

$$\hat{\boldsymbol{\Theta}}(s) = (\boldsymbol{V}^{\mathrm{T}}\boldsymbol{W}^g(s)\boldsymbol{V} + \lambda_g\boldsymbol{I})^{-1}(\boldsymbol{V}^{\mathrm{T}}\boldsymbol{W}^g(s)\boldsymbol{O} + \lambda_g\boldsymbol{\Theta}_0(s)) \tag{7}$$

where $\boldsymbol{I}$ is the identity matrix.

An important issue is tuning the value of λ_g as it controls the "degrees of transfer" for coefficients (parameters). The common way for tuning λ_g is grid search with cross-validation, which selects the optimal value of λ_g that has the best modeling performance evaluated by cross-validation from a specified grid of candidate values of λ_g (details can refer to Refs. [25] and [26]).

2.1.3 Estimate the Parameters of the Transfer-Learning-Based Geographically Weighted Regression Spatial Model. To estimate the coefficients of the GWR spatial model (see Eq. (2)) for the LDM measured surface, we first separate the coefficients into two parts. The first part is the spatially varying coefficients $\boldsymbol{\Gamma}$. The second part is the coefficients of the Gaussian process model and noise ε, which are denoted by $\boldsymbol{\theta}$. Then, after obtaining the coefficients $\boldsymbol{\Gamma}_0$ of the benchmark model for all target locations $\boldsymbol{S}$ using Eq. (4), a two-step algorithm can be employed to (1) estimate $\boldsymbol{\Gamma}$ for all target locations $\boldsymbol{S}$, then (2) estimate $\boldsymbol{\theta}$. The procedures are summarized in Algorithm 1.

Algorithm 1 Learning $\boldsymbol{\Gamma}$ and $\boldsymbol{\theta}$

Input: LDM surface height measurements $\boldsymbol{Z}$, covariates data $\boldsymbol{U}$, measurement locations $\boldsymbol{S}$, and $\boldsymbol{\Gamma}_0$ estimated by the HDM measured surface.
Output: $\boldsymbol{\Gamma}$ and $\boldsymbol{\theta}$.
Procedures:

1 Step (1): for every target location s, estimate $\boldsymbol{\Gamma}(s)$ based on Eqs. (6) and (7):

$$\hat{\boldsymbol{\Gamma}}(s) = (\boldsymbol{U}^T\boldsymbol{W}^g(s)\boldsymbol{U} + \lambda_g\boldsymbol{I})^{-1}(\boldsymbol{U}^T\boldsymbol{W}^g(s)\boldsymbol{Z} + \lambda_g\boldsymbol{\Gamma}_0(s))\,;$$

2 Use $\hat{\boldsymbol{\Gamma}}$ and $\boldsymbol{U}$ to calculate the estimated surface mean $\hat{\boldsymbol{Z}}_{mean}$ and the de-trended height data $\hat{\boldsymbol{Z}}_{sp}$ for every LDM measured locations using the following equation:

$$\hat{\boldsymbol{Z}}_{sp}(s) = \boldsymbol{Z}(s) - \hat{\boldsymbol{Z}}_{mean}(s) = \boldsymbol{Z}(s) - \boldsymbol{U}(s)\hat{\boldsymbol{\Gamma}}(s)\,;$$

3. Step (2): estimate $\boldsymbol{\theta}$ using dataset $\{\hat{\boldsymbol{Z}}_{sp}, \boldsymbol{S}\}$ (estimation method refers to Ref. [27]).

2.2 Region-Wise Regression Based Spatial Model. The GWR method models the nonstationarity by fitting regression models at every location, which result in high computational complexity. To reduce the computational complexity, the regression model can be fitted region-wise instead of point-wise, i.e., fit models independently within each of the regions. As such, the relationship between the covariate and the surface height is represented in piecewise nonstationary. Prior research has developed a lot of region-wise models, such as Bayesian treed Gaussian process model [28]. However, these models are not able to well capture the nonstationarity given only LDM measurements. To facilitate the use of transfer learning in building such a region-wise regression based spatial model, this section proposes the modeling of surface variations as follows:

$$Z(s) = \boldsymbol{U}(s)\boldsymbol{\Psi}(R_i|s \in R_i) + GP(s) + \varepsilon(s) \tag{8}$$

where $\boldsymbol{U}(s)\boldsymbol{\Psi}(R_i|s \in R_i)$ is the regression model for location s that belongs to region R_i; the partitioned k number of regions is denoted by $\boldsymbol{R} = \{R_1, R_2, \ldots, R_k\}$.

An important step for region-wise regression is to find the optimal spatial partitioning of $\boldsymbol{R} = \{R_1, R_2, \ldots, R_k\}$. In Sec. 2.2.1, we first present a spatial partitioning algorithm. Then, we propose a transfer learning method to train the model (Eq. (8)) for LDM measured surfaces.

2.2.1 Algorithm of Spatial Partitioning for Region-Wise Regression. Prior research has developed various partitioning algorithms, such as decision/regression tree [29], dynamic programming based algorithms, and greedy searching method [30]. This section develops a fast algorithm for spatial partitioning based on the greedy merging algorithm for segmented regression in Ref. [30]. See Algorithm 2.

For the nonstationary relationship with gradual change, there are no clear region boundaries, and the partitioning algorithm is likely to result in no partitioning. This is a major limitation of the proposed algorithm and the region-wise regression method.

Algorithm 2 Region-wise linear regression by greedy merging

Input: Dependent variable $\boldsymbol{O}$, independent variables $\boldsymbol{V}$, and variable locations $\boldsymbol{S}$.
Output: Partitioned regions $\boldsymbol{R} = \{R_1, R_2, \ldots, R_k\}$.
Procedures:

1. Make initial segmentations $\boldsymbol{R}^0$ on $\boldsymbol{S}$, e.g., uniformly partition the spatial area to k^0 rectangles, $\boldsymbol{R}^0 = \{R_1, R_2, \ldots, R_{k^0}\}$. Fit linear model of $\boldsymbol{O}$ and $\boldsymbol{V}$ within each region independently and obtain the sum of squared errors (SSE^0);
2. Iterate until $(SSE^i - SSE^{i-1})/SSE^{i-1} > T$ or $|\boldsymbol{R}^i| = 1$:
   (a) For all pairs of neighboring regions, evaluate the decrease or increase of SSE after merging a pair of neighboring regions, i.e., $\{SSE^i - SSE^{i-1}\}$;
   (b) Merge the pair of neighboring regions $\{R_u, R_v\}$ that result in the maximum decrease or minimum increase of SSE, i.e., $\boldsymbol{R}^i = \{\ldots, \cup\{R_u, R_v\}, \ldots\}$ and $k^i = |\boldsymbol{R}^i| = k^{i-1} - 1$.

Notes: i denotes the number of iteration. T is the stopping threshold that needs to be specified. This paper used $T = 0.05$. SSE can also be replaced with other metrics, such as the sum of absolute errors.

2.2.2 Development of Transfer Learning Based Region-Wise Regression. To build a region-wise regression model, the spatial partitioning for generating different regions is the first step and usually requires dense samplings over the entire spatial area. LDM measurements are not sufficient for partitioning a surface accurately. This section proposes the solution by assuming that the optimal spatial partitioning of a LDM measured surface is the same with that of historical HDM measured surfaces. This assumption is reasonable considering the discovered similar spatial nonstationarity of two surfaces shown in Fig. 4. Considering that the LDM measurement usually has only a few samples within each of the regions, this section proposes to help the regression within each of the regions using the following penalized solution:

$$\hat{\boldsymbol{\Theta}}(R_i) = \arg\min \frac{1}{2}(\boldsymbol{O}(R_i) - \boldsymbol{V}(R_i)\boldsymbol{\Theta}(R_i))^{\mathrm{T}}(\boldsymbol{O}(R_i) - \boldsymbol{V}(R_i)\boldsymbol{\Theta}(R_i)) + \frac{1}{2}\lambda_r\|\boldsymbol{\Theta}(R_i) - \boldsymbol{\Theta}_0(R_i)\|_2^2 \tag{9}$$

where the notations $\boldsymbol{O}, \boldsymbol{V}, \boldsymbol{\Theta}$ denote the same meanings with those in Eq. (6); R_i denotes the ith region of the entire partitioned surface $\boldsymbol{R} = \{R_1, R_2, \ldots, R_k\}$; $\boldsymbol{\Theta}_0(R_i)$ is the regression results of region R_i estimated using HDM data; λ_r is a tuning parameter that can be tuned by the same method presented in Sec. 2.1.2. The solution to Eq. (9) is given by

$$\hat{\boldsymbol{\Theta}}(R_i) = (\boldsymbol{V}(R_i)^{\mathrm{T}}\boldsymbol{V}(R_i) + \lambda_r\boldsymbol{I})^{-1}(\boldsymbol{V}(R_i)^{\mathrm{T}}\boldsymbol{O}(R_i) + \lambda_r\boldsymbol{\Theta}_0(R_i)) \tag{10}$$

where $\boldsymbol{I}$ is the identity matrix.

Notes: As for estimating the parameters of the transfer learning region-wise regression (tl-RR) spatial model (Eq. (8)), the procedures follow similar two steps as Algorithm 1, Sec. 2.1.3. The difference is with procedure 1 where tl-RR spatial model only needs to estimate a set of parameters for each region instead of that for the location. This section will not repeat the whole procedures.

2.3 Inference Rule Based Spatial Model. The region-wise regression based spatial model has limitations in dealing with the nonstationarity with gradual change. This section proposes a solution using fuzzy inference rule. Fuzzy inference is able to partition the surface into multiple areas with fuzzy boundaries, allowing for characterizing complex relationships by using several simple "if-then" rules with a better interpretability. An example can be found in Ref. [31]. It has been widely applied in many fields including medical image classification [32], geotechnical engineering [33], process modeling, monitoring and optimization [31,34–36], and control system [37,38]. Several different fuzzy inference models and model identification methods have been developed in

Refs. [39–44] among which adaptive network-based fuzzy inference system (ANFIS) [43,44] is the most commonly adopted methodology and is able to learn its parameters from training data. Thus, we propose an ANFIS-based surface variation model under the transfer learning framework. Based on Eq. (1), the model can be represented as the following equation:

$$Z(s) = \text{tl-ANFIS}(\boldsymbol{U}(s)) + \text{GP}(s) + \varepsilon(s) \tag{11}$$

where tl-ANFIS represents transfer-learning-based ANFIS.

Section 2.3.1 first reviews the ANFIS model. We further introduce the tl-ANFIS model and present the method to estimate the parameters of the tl-ANFIS based spatial model (Eq. (11)).

2.3.1 Review of the Adaptive Network-Based Fuzzy Inference System. Adaptive network-based fuzzy inference system is a five-layer feedforward network (see Fig. 6, benchmark ANFIS) and adopts Takagi-Sugeno fuzzy inference form [41]. For example, consider a first-order Sugeno fuzzy inference system, which contains two rules. Its "if-then" inference rules have the following format:

- Rule 1: If X is A_1 and Y is B_1, then $f_1 = p_1x + q_1y + r_1$.
- Rule 2: If X is A_2 and Y is B_2, then $f_2 = p_2x + q_2y + r_2$.

The corresponding fuzzy reasoning mechanism is shown in Fig. 5, where w is called "firing strength" measuring the degree, to which the rule matches the inputs, and output f is the weighted average of each rules' output. $\{A_1, B_1, A_2, B_2\}$ are the linguistic labels (e.g., small, large) associated with corresponding membership functions (see the Appendix). Since the ANFIS has a network-based structure, the premise parameters, i.e., parameters of the fuzzy membership functions $\{\mu(A_1), \mu(B_1), \mu(A_2), \mu(B_2)\}$, and consequent parameters $\{p_i, q_i, r_i\}$ can be learned by training dataset instead of being assigned subjectively. In this paper, the premise parameters are denoted by $\boldsymbol{\alpha}$, and the consequent parameters are denoted by $\boldsymbol{\beta}$.

It should be noted that the fuzzy inference such as ANFIS in this paper is not a simple aggregation of several subjective fuzzy rules as adopted in fuzzy logic. Instead, those "if-then" rules are carefully chosen and trained using training data. Also, ANFIS is essentially a region-wise model with fuzzy boundaries. The "if-then" rules reflect the partitioned regions for the input space. The membership functions and their premise parameters decide the positions and fuzzy boundaries of these regions. The consequent parameters can be regarded as the coefficients of the linear regression models for each region. As such, given the input of covariates and their corresponding coordinates, the ANFIS model is able to characterize the spatially varying relationship between the covariates and the surface height. For more technical details of ANFIS, see Refs. [43] and [44] and the Appendix.

2.3.2 Development of Transfer-Learning-Based Adaptive Network-Based Fuzzy Inference System. To train an ANFIS model, a commonly used learning algorithm named hybrid learning algorithm was proposed in Ref. [44]. However, the algorithm requires the training data to represent the features of input data thoroughly. For instance, the range of training data should cover the entire range of the input space, which makes the ANFIS model have a limited capability of extrapolation. Therefore, it is a challenge for a single surface with only LDM measurements to estimate a fine-tuned ANFIS model. To tackle the challenge, a transfer learning based algorithm is presented in this section to help build the ANFIS model for LDM measured surfaces.

First, an ANFIS model characterizing the nonstationary relationship between the covariate and the surface height is learned by the hybrid learning algorithm [44] using historical HDM data. Such ANFIS model learned using HDM data is called benchmark ANFIS model (see Ref. [44] for the detail procedures of the algorithm). Then, we assume that the ANFIS models for different surfaces have the same input membership functions (premise parameters α, layer 1), but different output functions (consequent parameters β, layer 4).

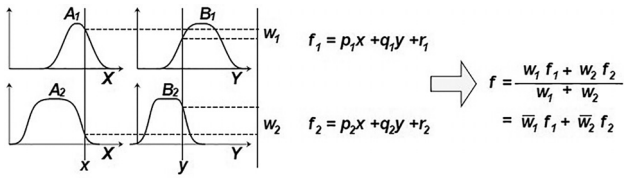

Fig. 5 Takagi-Sugeno fuzzy rules. Adapted from [44].

The assumed relationship between the benchmark ANFIS and the proposed tl-ANFIS is shown in Fig. 6. It can be seen that the knowledge inherited from the benchmark ANFIS is the number of fuzzy rules, layer 1, layer 2, and layer 3 (layers 2 and 3 are fixed). Such assumption essentially indicates that the surface models share the same pattern in region partitioning (see Sec. 2.3.1), which is validated by the similarity of the spatial nonstationarity as shown in Fig. 4. To estimate the consequent parameters of the tl-ANFIS model, a generalized least-squares estimation with regularization component is proposed in the following.

As shown in Fig. 6, the final output f' is represented as a linear combination of the consequent parameters given the values of premise parameters transferred from the benchmark ANFIS. The output f' in Fig. 6 can be written as follows:

$$\begin{aligned} f' &= \frac{w_1}{w_1 + w_2} f_1' + \frac{w_2}{w_2 + w_2} f_2' \\ &= \bar{w}_1 f_1' + \bar{w}_2 f_2' \\ &= (\bar{w}_1 x)p_1' + (\bar{w}_1 y)q_1' + (\bar{w}_1)r_1' + (\bar{w}_2 x)p_2' + (\bar{w}_2 y)q_2' + (\bar{w}_2)r_2' \\ &= \boldsymbol{X}\boldsymbol{\beta} \end{aligned} \tag{12}$$

which is a linear function with the consequent parameters $\boldsymbol{\beta}$, where $\boldsymbol{\beta} = [p_1', q_1', r_1', p_2', q_2', r_2']^{\mathrm{T}}$; $\boldsymbol{X} = [\bar{w}_1 x, \bar{w}_1 y, \bar{w}_1, \bar{w}_2 x, \bar{w}_2 y, \bar{w}_2]$. As a result, for an ANFIS model having M rules and P input variables with sample size N, the following regularized generalized least-squares estimation problem can be formulated to obtain the consequent parameters:

$$\hat{\boldsymbol{\beta}} = \arg\min \frac{1}{2}(\boldsymbol{Z} - \boldsymbol{X}\boldsymbol{\beta})^{\mathrm{T}}\boldsymbol{\Sigma}^{-1}(\boldsymbol{Z} - \boldsymbol{X}\boldsymbol{\beta}) + \frac{1}{2}\lambda_a \|\boldsymbol{\beta} - \boldsymbol{\beta}_0\|_2^2 \tag{13}$$

where $\boldsymbol{\beta}_0$ is the consequent parameters of the benchmark ANFIS model; $\boldsymbol{Z}$ is a vector of response observations with sample size N;

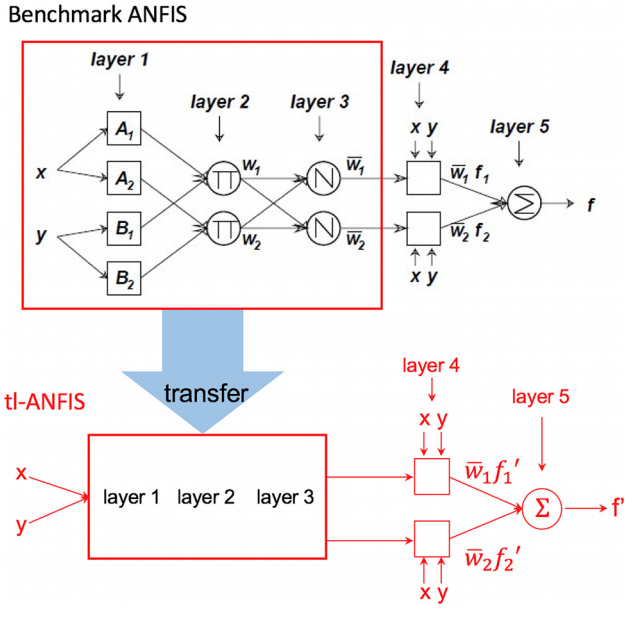

Fig. 6 Architecture of ANFIS and tl-ANFIS

$\boldsymbol{\Sigma}$ is the covariance matrix of the residuals; and λ_a is a tuning parameter that can be tuned by the same method presented in Sec. 2.1.2. The dimensions of $\boldsymbol{Z}$, $\boldsymbol{X}$, $\boldsymbol{\Sigma}$, and $\boldsymbol{\beta}$ are $N \times 1$, $N \times M(P+1)$, $N \times N$, and $M(P+1) \times 1$, respectively. The solution to Eq. (13) is given by

$$\hat{\boldsymbol{\beta}} = (\boldsymbol{X}^{\mathrm{T}}\boldsymbol{\Sigma}^{-1}\boldsymbol{X} + \lambda_a \boldsymbol{I})^{-1}(\boldsymbol{X}^{\mathrm{T}}\boldsymbol{\Sigma}^{-1}\boldsymbol{Z} + \lambda_a \boldsymbol{\beta}_0) \tag{14}$$

where $\boldsymbol{I}$ is the identity matrix.

2.3.3 Parameter Estimation for the Transfer-Learning-Based Adaptive Network-Based Fuzzy Inference System Based Spatial Model. The parameters of the tl-ANFIS based spatial model (see Eq. (11)) include those in the tl-ANFIS, the spatial Gaussian process, and white noise. This subsection presents the procedures for estimating these parameters.

The parameters of the benchmark ANFIS are first learned through the hybrid learning algorithm in Ref. [44] using the historical HDM data. Then, based on the proposed tl-ANFIS, the premise parameters of the benchmark ANFIS are treated as one part of the common information and will be transferred directly to the tl-ANFIS spatial model. The remaining nondirectly transferable parameters of the tl-ANFIS spatial model indicating the surface-to-surface difference are learned using two iterative steps including (1) estimation of the parameters of tl-ANFIS and (2) estimation of the parameters of GP and ε, until convergence. Usually, the convergence is achieved in less than three rounds of iteration.

Denote the nondirectly transferable consequent parameters of tl-ANFIS by $\boldsymbol{\beta}$, and denote the parameters of the spatial GP and noise ε by $\boldsymbol{\theta}$. The learning procedures are summarized in Algorithm 3. It should be noted that the generalized least-squares estimation (Eq. (14)) increases the computational complexity due to Σ. To reduce the computational complexity, ordinary least-squares can be used, i.e., eliminate Σ, and mostly will not impact the estimation a lot. Then, the algorithm needs no iteration and becomes a two-step algorithm that is similar to Algorithm 1.

Algorithm 3 Learning $\boldsymbol{\beta}$ and $\boldsymbol{\theta}$

Input: LDM surface height measurements $\boldsymbol{Z}$ and covariates data $\boldsymbol{U}$ at the same locations $\boldsymbol{S}$, and a benchmark ANFIS estimated by the HDM measured surface.
Output: $\boldsymbol{\beta}$ and $\boldsymbol{\theta}$.
Procedures:

1. Calculate the outputs for layer 1, layer 2, and layer 3 of the tl-ANFIS using input $[\boldsymbol{U}\,\boldsymbol{S}]$, and obtain $\boldsymbol{W} = \{\bar{w}_1, \bar{w}_2, \ldots, \bar{w}_M\}$, where M is the number of fuzzy rules (implementation details refer to Appendix);
2. Calculate $\boldsymbol{X}$ using $\boldsymbol{W}$, $\boldsymbol{U}$, and $\boldsymbol{S}$ via

$$\boldsymbol{X} = \boldsymbol{W} * \begin{bmatrix} [\boldsymbol{U}\,\boldsymbol{S}\,\boldsymbol{1}]_1 & & \\ & \ddots & \\ & & [\boldsymbol{U}\,\boldsymbol{S}\,1]_M \end{bmatrix} = \begin{bmatrix} \bar{w}_1[\boldsymbol{U}\,\boldsymbol{S}\,1] \\ \vdots \\ \bar{w}_M[\boldsymbol{U}\,\boldsymbol{S}\,1] \end{bmatrix}^T,$$

   where $[\boldsymbol{U}\,\boldsymbol{S}\,\boldsymbol{1}]$ is the matrix that combines process variables $\boldsymbol{U}$, coordinates of locations $\boldsymbol{S}$, and a column vector of a constant 1;
3. Initialize the covariance matrix $\boldsymbol{\Sigma}$ of residuals to identity matrix $\boldsymbol{I}$, and initialize $\boldsymbol{\beta}$ to zero matrix $\boldsymbol{0}$;
4. Estimate β based on Eqs. (13) and (14):

$$\hat{\boldsymbol{\beta}}^i = (\boldsymbol{X}^T\boldsymbol{\Sigma}^{-1}\boldsymbol{X} + \lambda_a \boldsymbol{I})^{-1}(\boldsymbol{X}^T\boldsymbol{\Sigma}^{-1}\boldsymbol{Z} + \lambda_a \boldsymbol{\beta}_0),$$

   where $\hat{\boldsymbol{\beta}}^i$ denotes the estimation of $\boldsymbol{\beta}$ at the ith iteration ($\hat{\boldsymbol{\beta}}^0 = 0$);
5. Use $\hat{\boldsymbol{\beta}}^i$ and $\boldsymbol{U}$ to calculate the estimated surface mean $\hat{\boldsymbol{Z}}_{mean}$ and the de-trended height data $\hat{\boldsymbol{Z}}_{sp}$:

$$\hat{\boldsymbol{Z}}_{sp} = \boldsymbol{Z} - \hat{\boldsymbol{Z}}_{mean} = \boldsymbol{Z} - tl\text{-}ANFIS(\boldsymbol{U}, \boldsymbol{S}|\hat{\boldsymbol{\beta}}^i);$$

6. Estimate $\boldsymbol{\theta}$ using dataset $\{\hat{\boldsymbol{Z}}_{sp}, \boldsymbol{S}\}$ (estimation method refers to Ref. [27]), and calculate the covariance matrix $\boldsymbol{\Sigma}$ of the residuals;
7. Repeat step 4 to step 6 until converge:

$$\|\boldsymbol{\beta}^i - \boldsymbol{\beta}^{i-1}\| < \delta_0,$$

   where δ_0 is a small positive threshold that is predetermined based on applications and accuracy requirements. It is chosen to be 0.1 for the case study.

2.4 Remarks on Transfer Learning Methods. *Remark 1: Method comparisons*. This paper has discussed three models that can characterize nonstationarity for abrupt or gradual changes in the covariate-surface height relationship by conducting point-wise, region-wise, and fuzzy region-wise modeling. GWR estimates a set of parameters at every location of interest using weighted least squares. Therefore, it is computationally complex. By contrast, RR and ANFIS have fewer parameters and are more computationally efficient. As mentioned earlier, the type of nonstationarity can be either an abrupt change or gradual change. GWR uses a weight function to capture the coefficient change, which makes the estimated coefficients change smoothly (gradually). RR estimates model coefficients independently within each region. Thus, the estimated coefficients would exhibit piece-wise patterns with an abrupt change. ANFIS partitions the input space using regions with fuzzy boundaries, and it usually results in smooth (gradual) transitions between different regions. Table 2 summarizes the nonstationary patterns that three models can capture along with computational complexity (assume that tl-ANFIS uses ordinary least-squares instead of generalized least-squares) under the transfer learning framework.

Remark 2: Applicable conditions of transfer learning. It should be noted that the transfer learning can improve the modeling of surface variations only when the nonstationarity are similar such as shown in Fig. 4. If the nonstationary relationship is highly influenced by other incontrollable and unobservable manufacturing factors, the similarity assumption might be violated due to the intractable change of these factors, potentially causing negative knowledge transfer and jeopardizing surface modeling accuracy. We would recommend the following guidelines to mitigate potential negative knowledge transfer. First, it is advisable to include the data of machined surfaces from the same type of manufacturing line because the machine settings are mostly the same. Second, for surface shape modeling, we should choose covariates to be those that significantly impact axial cutting force, a universal factor contributing to the generation of surface shape variations. The prior research [1,15] on HDM surface data modeling reported that in normal surface manufacturing processes, the axial cutting force variations are mostly affected by the MRR and the number of cutter insert engagement. The surface variation patterns induced by the two variables (covariates) can account for a significant percent of surface flatness errors. As such, using these variables as covariates can reduce the likelihood of the negative knowledge transfer since their impacts on surface shape variations are similar across multiple surface machining processes. Third, the similarity of covariate-surface height relationship can be compared for different parts such as Fig. 4 before employing transfer learning.

Remark 3: Covariate selection. If multiple covariates play unknown and unequal roles in affecting the surface height variations, selecting the covariates that significantly affect the generation of surface variations is necessary. The covariate selection can be achieved by adopting the commonly used variable selection methods, e.g., lasso method [25] for GWR and region-wise regression, backward selection method [45] for ANFIS.

Table 2 Theoretical comparisons of three methods (where O is "big O notation" measuring the asymptotic running time of an algorithm)

	GWR	RR	ANFIS
Complexity	$O(N^2)$	$O(N)$	$O(N)$
Gradual change	✓		✓
Abrupt change		✓	

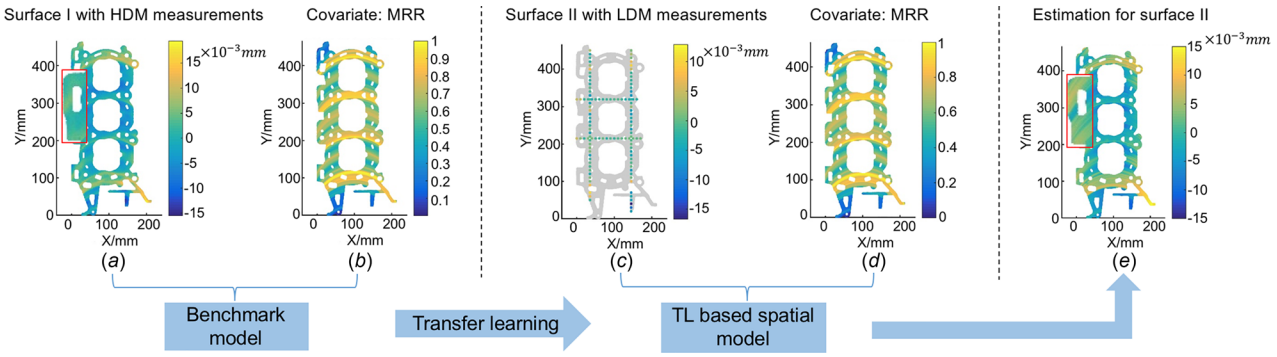

Fig. 7 Logic of transfer learning (TL)-based spatial modeling for an engine head surface: (*a*) HDM measurements for surface I (partial enlarged detail shown in the box); (*b*) normalized MRR for surface I; (*c*) LDM measurements for surface II; (*d*) normalized MRR for surface II; and (*e*) modeling of surface II using TL-based spatial model (partial enlarged detail shown in the box)

Table 3 Surface modeling results of case A (RMSE unit: × 10^{-3} mm)

Method	RMSE
tl-GWR spatial	2.43
tl-RR spatial	3.69
tl-ANFIS spatial	2.15
CK	4.04
OK	5.26

3 Case Studies

Two real-world case studies were conducted to compare and demonstrate the advantages of the proposed transfer learning based methods. The correlation-enabled spatial model in Ref. [16] (denoted as CK) and ordinary Kriging (denoted as OK) model were employed as the comparison benchmark. An exponentiation kernel function was used for the GP model (see Eq. (15)). The root-mean-square error (RMSE) is used as the metric to evaluate the modeling performance

$$k(s_i, s_j) = c_f \exp\left(-\frac{\|s_i - s_j\|}{c_l}\right) + c_n \delta_{i,j} \tag{15}$$

where $\delta_{i,j}$ is the Kronecker delta function; and c_f, c_l, and c_n are unknown coefficients to be estimated.

It is worth noting that this paper focuses on the modeling of surface height in lateral resolution and does not consider the effect of different vertical resolution of HDM and LDM. The modeling of surface height in vertical resolution can refer to Ref. [46]. As such, without loss of generality, the case studies in this section simulated the CMM measurements (LDM measurements) via selecting sparser samples from HDM measurements.

3.1 Case A: Surface Variation Modeling for Automotive Engine Head Deck Faces. The methods were applied to modeling the surface variations for automotive engine head deck faces. A laser holographic interferometer was employed to measure two engine head surfaces (denoted as surface I and surface II) at high resolution (lateral:150 μm and vertical 0.1 μm)(see Fig. 7(*a*)) in an automotive engine plant. A subset of these measurements is sampled as CMM measurements (see Fig. 7(*c*)). For a metal workpiece with a bulky volume such as engine head/blocks, the effect of fixture clamping on surface flatness is insignificant. Additionally, the optical metrology system employed in-plant has limited resolution in characterizing the surface texture such as roughness. Thus, the effects of fixturing and spindle dynamics are not considered. The process variables that impact surface shapes due to axial cutting force variations such as MRR and cutting insert engagement are included as covariates in the case studies. In particular, case A uses the MRR as the only covariate since the number of cutter insert engagement does not significantly change over the engine surface (see Figs. 7(*b*) and 7(*d*)).

To enable the transfer learning, we use the HDM measurements and MRR data from the surface I to build the benchmark GWR/RR/ANFIS model. The LDM measurements (CMM measurements) and MRR data from the surface II are then used to update the GWR/RR/ANFIS model. The logic is also outlined by the arrows in Fig. 7.

The model RMSEs for surface II of all the five methods are shown in Table 3. As can be seen from the results, the modeling

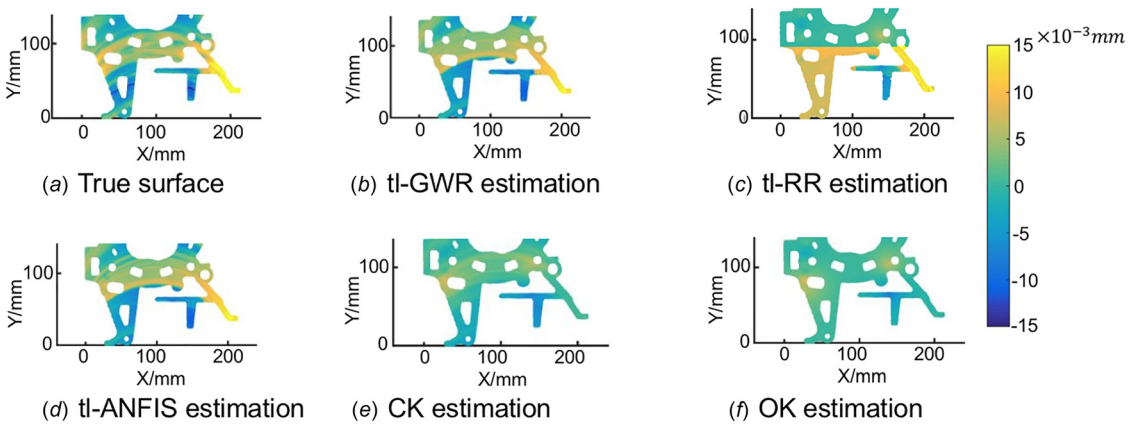

Fig. 8 Modeling results of tail sections on surface II versus true data for the engine head deck face. It can be seen that the proposed methods (*b*) and (*d*) achieve an estimation closer to the true data (*a*) compared with a state-of-the-art method (*e*) and a commonly used method (*f*). Method (*c*) estimates bad at the left tail section.

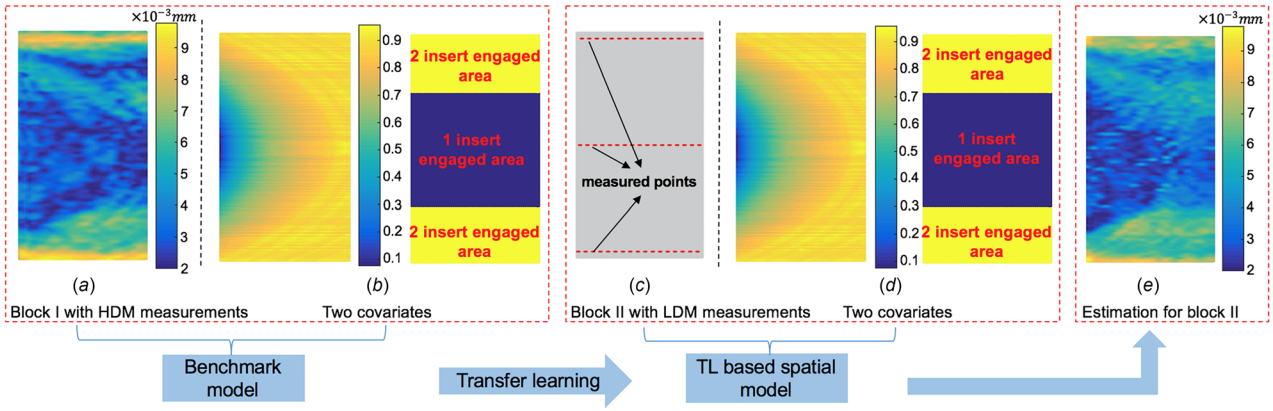

Fig. 9 Logic of TL-based spatial modeling for the block surface: (*a*) HDM measurements for block I; (*b*) normalized MRR and the number of insert-engagement for block I; (*c*) LDM measurements for block II; (*d*) normalized MRR and the number of insert-engagement for block II; and (*e*) modeling of block II using TL-based spatial model

Table 4 Surface modeling results of case B (RMSE unit: × 10^{-3} mm)

Method	RMSE
tl-GWR spatial	0.85
tl-RR spatial	0.92
tl-ANFIS spatial	0.83
CK	1.69
OK	1.37

accuracy is improved by 54%, 30%, 59%, and 23% through data fusion methods, i.e., tl-GWR, tl-RR, tl-ANFIS, and CK, respectively, compared with the method with no data fusion (OK). The improvement brought by the data fusion methods can be visualized in Fig. 8, which shows the true and the estimated surface height of a partial area in surface II. It can be seen that the tl-ANFIS spatial model and the tl-GWR spatial model successfully captured the surface height variations and showed significant improvement over the OK model. However, the proposed tl-RR spatial model showed bad estimations at this tail section, especially the left tail section. The reason for causing the bad estimations was the nonstationary relationship of MRR-surface height changed gradually instead of abruptly, and the piece-wise assumption of tl-RR did not hold. Due to the nonstationary relationship between the surface height and MRR, state-of-the-art CK method failed to characterize the surface height variations accurately and showed only limited improvement over the OK model. In summary, incorporating the nonstationary relationship would greatly improve the modeling accuracy, and the transfer learning framework plays a key role in building those models that are modeling nonstationarity.

3.2 Case B: A Surface Milling Experiment. Two solid blocks of aluminum 2024-T351 with dimensions of $75 \times 270 \times 75\,\text{mm}^3$ were cut in a face milling operation, which were used by our prior study [15]. The depth of cut is 0.5 mm, the feed rate is 0.5 mm/tooth, and the spindle speed is 1000 rpm. The cutter has an effective diameter of 101.6 mm with five inserts. The face milling operation was implemented on a Cincinnati computer numerical control machine (model HMC-400EP), and the machined surfaces were measured by a Shapix laser holographic interferometer, an HDM system for surfaces. One block is used to train the benchmark model and the other is used for model validation. The surface measurements, two covariates, and down-sampled surface data to simulate LDM measurements are shown in Fig. 9. Panel (*a*) shows the HDM surface measurement for block I used for training the benchmark model. Panel (*b*) shows the two covariates, MRR and the number of cutter inset engagement, when machining block I. LDM data were generated via downsampling from the HDM data of block II. The sampling positions are shown in panel (*c*). The covariates for block II are shown in panel (*d*). Figure 9 also outlines the logic of the transfer learning from block I to block II.

The modeling RMSEs for block II are summarized in Table 4. Compared with CK and OK, the proposed transfer learning based methods greatly improved the modeling accuracy. Concerning RMSE, the improvements of the three methods over OK method are 38%, 33%, and 39%, respectively. Figure 10 compares the modeled surface variations and demonstrates that the proposed tl-GWR, tl-RR, and tl-ANFIS achieved better estimations of surface variations compared with CK and OK. It should be noted that the correlation-enabled spatial model (CK) developed in the prior research gives misleading overall correlation information due to the nonstationary relationships, making the estimation even worse than OK. It is also noticed that tl-RR method did not make significant worse estimations than tl-GWR and tl-ANFIS as it did for case A. The reason for the improvement is that the introducing of

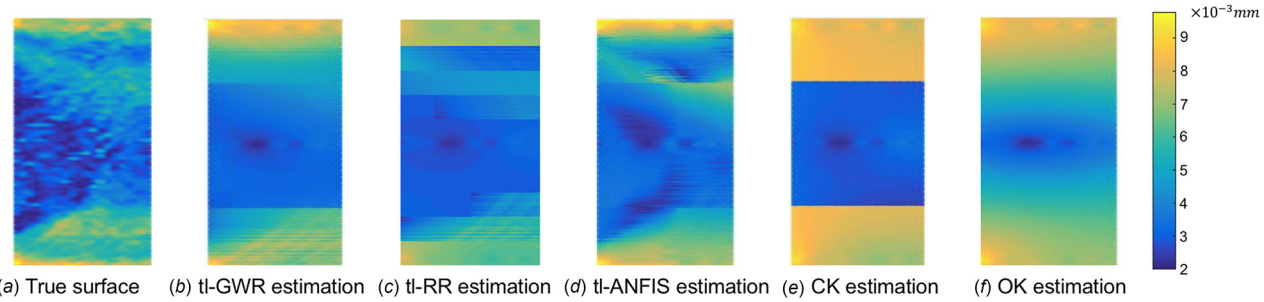

Fig. 10 Surface modeling results for block II. The results show that the proposed tl-GWR (*b*), tl-RR(*c*), and tl-ANFIS (*d*) achieve the estimation closer to the true data (*a*) compared with a state-of-the-art method (*e*) and a commonly used method (*f*).

a categorical covariate, i.e., the number of insert engagement, makes the nonstationary relationship change less smoothly.

4 Conclusions

This paper solves a problem of improving surface variation estimation based on LDM surface data regularly measured in-plant by fusing historical HDM surface data that have limited availability. The idea of fusion is to first extract spatial surface variation patterns that reflect common cutting force dynamics in surface milling operations from the HDM data and then transfer the information on the patterns to a target surface of interest that is only measured by LDM. The surface variation patterns extracted from the HDM data are characterized by a number of covariates that are correlated to surface height. The knowledge transfer is enabled by the same impact of covariates on the surface height across multiple surface machining processes. Such a relationship between the covariate and the surface height can vary over different surface areas, exhibiting strong spatial nonstationarity. The spatial nonstationarity can significantly affect the surface modeling accuracy. To deal with the nonstationarity challenges in the fusion of LDM and HDM data problem, this paper develops three spatial models under a transfer learning framework, including a point-wise local regression based spatial model (tl-GWR spatial model), region-wise regression based spatial model (tl-RR spatial), and fuzzy-region-wise inference rule based spatial model (tl-ANFIS spatial model). The tl-GWR is straightforward in dealing with spatial nonstationarity, which conducts weighted regression for every location. GWR can deal with nonstationarity with gradual change; however, it may introduce a large number of model parameters and increase computational complexity. The two region-wise models (tl-RR and tl-ANFIS) have fewer parameters and are more computationally efficient than tl-GWR among which the tl-RR deals with nonstationarity with abrupt change and the tl-ANFIS deals with nonstationarity with gradual change and even nonlinearity.

Two real-world case studies using automotive engine head deck face measurements and a surface milling experiment were conducted to compare the proposed methods with a traditional Kriging model based on statistical interpolation/extrapolation and a state-of-the-art correlation-enabled spatial model. The results demonstrated that the proposed tl-ANFIS and tl-GWR methods could achieve significant improvement in surface variation modeling compared with the two previous methods. The proposed tl-RR method also improved the modeling accuracy but with less amount of improvement than tl-ANFIS and tl-GWR, because the spatial nonstationarity of the two cases were of gradual change. It is noticeable that the correlation-enabled model even generates worse RMSE due to a lack of consideration of nonstationarity relationship. Therefore, we can conclude that incorporating nonstationarity can greatly improve the modeling accuracy of surface variations, and transfer learning is an effective method in building those nonstationarity involved models with inadequate data. For the three proposed models, we can conclude that tl-ANFIS spatial model is the best solution for these two cases regarding the modeling accuracy and computational efficiency. The tl-RR spatial model could be employed when the discovered nonstationarity is of abrupt change. The tl-GWR spatial model can be used as an alternative to the tl-ANFIS model when the number of estimating locations is not large. The transfer learning methods considering nonstationarity provide guidelines for in-plant quality control for surface machining processes by cost-effectively utilizing multiresolution data to improve surface variation monitoring. The proposed methods also have the potential to be applied to other processes where multiresolution data are measured, and a common nonstationary relationship between the independent variables and response can be discovered.

Acknowledgment

This research was supported by National Science Foundation. The authors also thank Coherix, Inc., for identifying industry problems in surface machining process control and providing valuable surface data measured from their customers in an engine manufacturing plant.

Funding Data

- Division of Civil, Mechanical and Manufacturing Innovation (1744131 and CMMI-1434411).

Appendix: Adaptive Network-Based Fuzzy Inference System Model Layer by Layer

As can be seen from Fig. 6, assume that we have two input variables x and y, and one response variable f, the description of ANFIS is given as follows:

- *Layer 1:* This layer specifies the membership function for every input variable

$$L_i^1 = \mu_{A_i}(x) \tag{A1}$$

  where L denotes node function which is membership function in *layer 1*, x is the input to node i, and A_i is the linguistic label (e.g., small, large) associated with membership function μ_{A_i}. A commonly used Gaussian membership function is as follows:

$$\mu_{A_i}(x) = e^{\frac{-(x-c_i)^2}{2a_i^2}} \tag{A2}$$

  where $\{a_i, c_i\}$ is the parameter set for node i in layer 1. The parameters in this layer are called premise parameters.
- *Layer 2:* Every node in this layer is a fixed operator Π which multiplies the incoming memberships from layer 1

$$w_i = \mu_{Ai}(x) \times \mu_{Bi}(y), \quad i = 1, 2 \tag{A3}$$

  where w denotes the "firing strength" of a fuzzy rule.
- *Layer 3:* Every node in this layer is a fixed operator N calculating the weight of the ith rule for input x and y which is called "normalized firing strength"

$$\bar{w}_i = \frac{w_i}{w_1 + w_2}, \quad i = 1, 2 \tag{A4}$$

- *Layer 4:* Every node in this layer has the following node function:

$$L_i^4 = \bar{w}_i f_i = \bar{w}_i(p_i x + q_i y + r_i) \tag{A5}$$

  where $\{p_i, q_i, r_i\}$ is the parameter set. The parameters in this layer are called consequent parameters.
- *Layer 5:* The node in this layer is a fixed operator Σ which calculates the final output as the summation of outputs from *layer 4*

$$L_1^5 = f = \sum_i \bar{w}_i f_i = \frac{\sum_i w_i f_i}{\sum_i w_i} \tag{A6}$$

References

[1] Nguyen, H. T., Wang, H., Tai, B. L., Ren, J., Hu, S. J., and Shih, A., 2016, "High-Definition Metrology Enabled Surface Variation Control by Cutting Load Balancing," ASME J. Manuf. Sci. Eng., **138**(2), p. 021010.

[2] Ren, J., Park, C., and Wang, H., 2018, "Stochastic Modeling and Diagnosis of Leak Areas for Surface Assembly," ASME J. Manuf. Sci. Eng., **140**(4), p. 041011.

[3] Shao, Y., Yin, Y., Du, S., Xia, T., and Xi, L., 2018, "Leakage Monitoring in Static Sealing Interface Based on Three Dimensional Surface Topography Indicator," ASME J. Manuf. Sci. Eng., **140**(10), p. 101003.
[4] Du, S., Liu, C., and Xi, L., 2015, "A Selective Multiclass Support Vector Machine Ensemble Classifier for Engineering Surface Classification Using High Definition Metrology," ASME J. Manuf. Sci. Eng., **137**(1), p. 011003.
[5] Wells, L. J., Shafae, M. S., and Camelio, J. A., 2016, "Automated Surface Defect Detection Using High-Density Data," ASME J. Manuf. Sci. Eng., **138**(7), p. 071001.
[6] Zhu, X., Ding, H., and Wang, M. Y., 2004, "Form Error Evaluation: An Iterative Reweighted Least Squares Algorithm," ASME J. Manuf. Sci. Eng., **126**(3), pp. 535–541.
[7] Yang, B.-D., and Menq, C.-H., 1993, "Compensation for Form Error of End-Milled Sculptured Surfaces Using Discrete Measurement Data," Int. J. Mach. Tools Manuf., **33**(5), pp. 725–740.
[8] Grove, D. M., Woods, D. C., and Lewis, S. M., 2004, "Multifactor b-Spline Mixed Models in Designed Experiments for the Engine Mapping Problem," J. Qual. Technol., **36**(4), pp. 380–391.
[9] Jung, H., and Kim, K., 2000, "A New Parameterisation Method for Nurbs Surface Interpolation," Int. J. Adv. Manuf. Technol., **16**(11), pp. 784–790.
[10] Suriano, S., Wang, H., and Hu, S. J., 2012, "Sequential Monitoring of Surface Spatial Variation in Automotive Machining Processes Based on High Definition Metrology," J. Manuf. Syst., **31**(1), pp. 8–14.
[11] Yang, T.-H., and Jackman, J., 2000, "Form Error Estimation Using Spatial Statistics," ASME J. Manuf. Sci. Eng., **122**(1), pp. 262–272.
[12] Xia, H., Ding, Y., and Wang, J., 2008, "Gaussian Process Method for Form Error Assessment Using Coordinate Measurements," IIE Trans., **40**(10), pp. 931–946.
[13] Jin, R., Chang, C.-J., and Shi, J., 2012, "Sequential Measurement Strategy for Wafer Geometric Profile Estimation," IIE Trans., **44**(1), pp. 1–12.
[14] Yang, Y., and Shao, C., 2018, "Spatial Interpolation for Periodic Surfaces in Manufacturing Using a Bessel Additive Variogram Model," ASME J. Manuf. Sci. Eng., **140**(6), p. 061001.
[15] Nguyen, H. T., Wang, H., and Hu, S. J., 2013, "Characterization of Cutting Force Induced Surface Shape Variation in Face Milling Using High-Definition Metrology," ASME J. Manuf. Sci. Eng., **135**(4), p. 041014.
[16] Suriano, S., Wang, H., Shao, C., Hu, S. J., and Sekhar, P., 2015, "Progressive Measurement and Monitoring for Multi-Resolution Data in Surface Manufacturing Considering Spatial and Cross Correlations," IIE Trans., **47**(10), pp. 1033–1052.
[17] Shao, C., Ren, J., Wang, H., Jin, J. J., and Hu, S. J., 2017, "Improving Machined Surface Shape Prediction by Integrating Multi-Task Learning With Cutting Force Variation Modeling," ASME J. Manuf. Sci. Eng., **139**(1), p. 011014.
[18] Du, S., and Fei, L., 2016, "Co-Kriging Method for Form Error Estimation Incorporating Condition Variable Measurements," ASME J. Manuf. Sci. Eng., **138**(4), p. 041003.
[19] Cheng, C., Sa-Ngasoongsong, A., Beyca, O., Le, T., Yang, H., Kong, Z., and Bukkapatnam, S. T., 2015, "Time Series Forecasting for Nonlinear and Non-Stationary Processes: A Review and Comparative Study," IIE Trans., **47**(10), pp. 1053–1071.
[20] Pan, S. J., and Yang, Q., 2010, "A Survey on Transfer Learning," IEEE Trans. Knowl. Data Eng., **22**(10), pp. 1345–1359.
[21] Duvenaud, D. K., Nickisch, H., and Rasmussen, C. E., 2011, "Additive Gaussian Processes," Advances in Neural Information Processing Systems, pp. 226–234.
[22] Rue, H., and Held, L., 2005, *Gaussian Markov Random Fields: Theory and Applications*, CRC Press, Boca Raton, FL.
[23] Fotheringham, A. S., Brunsdon, C., and Charlton, M., 2002, *Geographically Weighted Regression: The Analysis of Spatially Varying Relationships*, Wiley, New York.
[24] Hoerl, A. E., and Kennard, R. W., 1970, "Ridge Regression: Biased Estimation for Nonorthogonal Problems," Technometrics, **12**(1), pp. 55–67.
[25] Tibshirani, R., 1996, "Regression Shrinkage and Selection Via the Lasso," J. R. Stat. Soc. Ser. B (Methodol.), **58**(1), pp. 267–288.
[26] Zou, H., and Hastie, T., 2005, "Regularization and Variable Selection Via the Elastic Net," J. R. Stat. Soc.: Ser. B (Stat. Methodol.), **67**(2), pp. 301–320.
[27] Rasmussen, C. E., 2004, "Gaussian Processes in Machine Learning," *Advanced Lectures on Machine Learning*, Springer, Berlin, pp. 63–71.
[28] Gramacy, R. B., and Lee, H. K. H., 2008, "Bayesian Treed Gaussian Process Models With an Application to Computer Modeling," J. Am. Stat. Assoc., **103**(483), pp. 1119–1130.
[29] Breiman, L., 2017, *Classification and Regression Trees*, Routledge, New York.
[30] Acharya, J., Diakonikolas, I., Li, J., and Schmidt, L., 2016, "Fast Algorithms for Segmented Regression," 33rd International Conference on Machine Learning (ICML), New York, June 19–24, pp. 2878–2886.
[31] Lih, W.-C., Bukkapatnam, S. T., Rao, P., Chandrasekharan, N., and Komanduri, R., 2008, "Adaptive Neuro-Fuzzy Inference System Modeling of MRR and WIWNU in CMP Process With Sparse Experimental Data," IEEE Trans. Autom. Sci. Eng., **5**(1), pp. 71–83.
[32] Hosseini, M. S., and Zekri, M., 2012, "Review of Medical Image Classification Using the Adaptive Neuro-Fuzzy Inference System," J. Med. Signals Sens., **2**(1), pp. 49–60.
[33] Cabalar, A. F., Cevik, A., and Gokceoglu, C., 2012, "Some Applications of Adaptive Neuro-Fuzzy Inference System (ANFIS) in Geotechnical Engineering," Comput. Geotech., **40**, pp. 14–33.
[34] Chang, S., and Aw, C., 1996, "A Neural Fuzzy Control Chart for Detecting and Classifying Process Mean Shifts," Int. J. Prod. Res., **34**(8), pp. 2265–2278.
[35] Mesina, O. S., and Langari, R., 2001, "A Neuro-Fuzzy System for Tool Condition Monitoring in Metal Cutting," ASME J. Manuf. Sci. Eng., **123**(2), pp. 312–318.
[36] Ubaid, A. M., Dweiri, F. T., Aghdeab, S. H., and Al-Juboori, L. A., 2018, "Optimization of Electro Discharge Machining Process Parameters With Fuzzy Logic for Stainless Steel 304 (ASTM A240)," ASME J. Manuf. Sci. Eng., **140**(1), p. 011013.
[37] Aguilar, L., Melin, P., and Castillo, O., 2003, "Intelligent Control of a Stepping Motor Drive Using a Hybrid Neuro-Fuzzy ANFIS Approach," Appl. Soft Comput., **3**(3), pp. 209–219.
[38] Ou, X., Arinez, J., Chang, Q., and Xiao, G., 2017, "Cost Analysis and Fuzzy Control for Collapsible Container Usage Based on Closed-Loop Supply Chain Model," ASME J. Manuf. Sci. Eng., **139**(8), p. 081005.
[39] Wang, L.-X., and Mendel, J. M., 1992, "Back-Propagation Fuzzy System as Nonlinear Dynamic System Identifiers," IEEE International Conference on Fuzzy Systems, San Diego, CA, Mar. 8–12, pp. 1409–1418.
[40] Yager, R. R., and Filev, D. P., 1994, "Generation of Fuzzy Rules by Mountain Clustering," J. Intell. Fuzzy Syst.: Appl. Eng. Technol., **2**(3), pp. 209–219.
[41] Takagi, T., and Sugeno, M., 1985, "Fuzzy Identification of Systems and Its Applications to Modeling and Control," IEEE Trans. Syst. Man Cybern., (1), pp. 116–132.
[42] Chiu, S. L., 1994, "Fuzzy Model Identification Based on Cluster Estimation," J. Intell. Fuzzy Syst., **2**(3), pp. 267–278.
[43] Jang, J.-S. R., 1991, "Fuzzy Modeling Using Generalized Neural Networks and Kalman Filter Algorithm," AAAI J., **2**, pp. 762–767.
[44] Jang, J.-S. R., 1993, "ANFIS: Adaptive-Network-Based Fuzzy Inference System," IEEE Trans. Syst. Man Cybern., **23**(3), pp. 665–685.
[45] Chiu, S. L., 1996, "Selecting Input Variables for Fuzzy Models," J. Intell. Fuzzy Syst., **4**(4), pp. 243–256.
[46] Xia, H., Ding, Y., and Mallick, B. K., 2011, "Bayesian Hierarchical Model for Combining Misaligned Two-Resolution Metrology Data," IIE Trans., **43**(4), pp. 242–258.